Algebraic probability density tails in decaying isotropic two-dimensional turbulence

Javier Jiménez

Journal of Fluid Mechanics / Volume 313 / April 1996, pp 223 - 240
DOI: 10.1017/S0022112096002194, Published online: 26 April 2006

J. Fluid Mech. (1996), *vol.* 313, *pp.* 223–240

Algebraic probability density tails in decaying isotropic two-dimensional turbulence

By JAVIER JIMÉNEZ

School of Aeronautics, Pl. Cardenal Cisneros 3, 28040 Madrid, Spain

(Received 21 August 1995 and 15 December 1995)

The p.d.f. of the velocity gradients in two-dimensional decaying isotropic turbulence is shown to approach a Cauchy distribution, with algebraic s^{-2} tails, as the flow becomes dominated by a large number of compact coherent vortices. The statistical argument is independent of the vortex structure, and depends only on general scaling properties. The same argument predicts a Gaussian p.d.f. for the velocity components. The convergence to these limits as a function of the number of vortices is analysed. It is found to be fast in the former case, but slow (logarithmic) in the latter, resulting in residual u^{-3} tails in all practical cases. The influence of a spread Gaussian vorticity distribution in the cores is estimated, and the relevant dimensionless parameter is identified as the area fraction covered by the cores. A comparison is made with the result of numerical simulations of two-dimensional decaying turbulence. The agreement of the p.d.f.s is excellent in the case of the gradients, and adequate in the case of the velocities. In the latter case the ratio between energy and enstrophy is computed, and agrees with the simulations. All the one-point statistics considered in this paper are consistent with a random arrangement of the vortex cores, with no evidence of energy screening.

1. Introduction

Two-dimensional turbulence constitutes a convenient, simpler, model to test ideas which may be applicable to turbulent flows in general. While there is no question that two- and three-dimensional flows are different, the decay of two-dimensional random initial conditions at high Reynolds numbers shares with 'real' three-dimensional turbulence many characteristics, such as chaotic behaviour, mixing, and a large number of degrees of freedom. It is therefore of interest that the behaviour of both systems is similar in some other respects, specially when it can be analysed better in one case than in the other. Although it may not be clear at the moment how to extend such analysis to the other case, the hope is that the methods which are successful in one might be of some use in the other when, and if, more information becomes available. In this paper we deal with the problem of the intermittent behaviour of one-point statistics. We will show that much can be derived for them in two-dimensional decaying turbulence, using a simple dynamical model and statistical arguments of purely kinematic nature.

The presence of strongly intermittent probability distributions for the velocity gradients is characteristic of most turbulent flows at high Reynolds numbers (Batchelor & Townsend 1949; Anselmet *et al.* 1984; Castaing, Gagne & Hopfinger 1990). Their deviation from Gaussian is conveniently expressed in terms of their flatness factors,

which are known to behave in a way that may be consistent with unbounded moments in the inviscid limit (Van Atta & Antonia 1980).

Attempts to explain this behaviour in terms of a structural description of the flow range from simple estimates (Townsend 1951) to the very sophisticated calculation in Pullin & Saffman (1993). The latter contains a good historical overview of the subject. Their success has been mixed, and they generally need at least one adjustable parameter to compensate for the incomplete knowledge of the details of the three-dimensional turbulent structure.

Most theoretical discussions on intermittency have been purely statistical, emphasizing the functional form of the probability density functions (p.d.f.s) of the different variables, and advancing models to explain them in terms of the global properties of the Euler equations (Kolmogorov 1962; Obukhov 1962; Gurvitch & Yaglom 1967; Novikov 1971; Parisi & Frisch 1985; Meneveau & Sreenivasan 1991). While the physical ideas behind these models are reasonable, they do not fully constrain the p.d.f.s, and most of them have to rely on phenomenological approximations to the experimental observations. A popular model that fits the tails of most observed distributions is the stretched exponential $p(x) \sim \exp(-cx^{\beta})$, where c and β generally depend on the Reynolds number (She 1991; Kailsanath, Sreenivasan & Stolovitzky 1992).

All the statistical moments, $\mu_n = \int x^n p(x)\,\mathrm{d}x$, of stretched exponentials are finite, but they become larger as the 'stretching' exponent β decreases, as it appears to do for turbulent gradients when the Reynolds number increases (see the references above). Distributions with algebraic tails have moments which are infinite beyond a given order, and the presence of very large flatness factors suggests that algebraic tails may appear in turbulence as the inviscid limit of the stretched exponentials. In fact algebraic probability distributions have been suggested on theoretical grounds for very intermittent distributions of the energy dissipation (Mandelbrot 1974).

Recent numerical simulations have provided direct observations of the geometry of a particular fraction of the intermittent vorticity field which, in three-dimensional flows, is organized in the form of filaments (Siggia 1981; Kerr 1985; Hosokawa & Yamamoto 1990; She, Jackson & Orszag 1990; Ruetsch & Maxey 1991; Vincent & Meneguzzi 1991; Jiménez *et al.* 1993), raising the hope that the p.d.f.s could be derived directly from the kinematic properties of the filaments. That hope is still unfulfilled, because the filaments constitute only a small part of the flow, and the organization of the rest of the vorticity has to be understood before a full theory can be formulated.

While the experiments quoted above deal with three-dimensional flows, very pronounced intermittency effects are also observed in two-dimensional isotropic decaying turbulence. The modelling situation is in this case different from the one in three dimensions, since it has been known for some time that the vorticity becomes concentrated into compact coherent structures that dominate the flow, which is otherwise mostly irrotational (Brachet *et al.* 1988; Santangelo, Benzi & Legras 1989; McWilliams 1990).

From this simple dynamical model it is possible to predict the form of the p.d.f.s for both the velocity and the velocity gradients, thereby linking the statistical and structural descriptions of at least this simple turbulent flow but, to our knowledge, that has not been attempted up to now. The purpose of this paper is to study this connection.

It is clear that the probability distributions of the strongest gradients and velocities depend on the details of the vorticity distribution within the compact vortices, and on

their strength and number, but we will show below that the same is not true for the irrotational velocity gradients in the background which, since the vortices fill only a small fraction of the total area, is responsible for most of the integrated probability. It will turn out that those p.d.f.s have algebraic tails.

In the spirit of the first paragraph of this Introduction, we consider only two-dimensional flows, for which there is a reasonable consensus on the flow structure. The probability distributions for the gradients and for the velocity components are treated first in the limit of infinitely many point vortices. The effect of the finite number of vortices is then analysed and found to be negligible for the distribution of the gradients, but important for the velocities. Finally the corrections due to spread vortex cores are estimated, and the results compared to numerical simulations of decaying, high Reynolds number, two-dimensional turbulence.

2. Point vortices

Consider a two-dimensional flow field dominated by vortices whose characteristic vorticity and radius are ω_0 and R, separated by an average distance D. The mean-squared vorticity, which is kinematically proportional to the mean-squared velocity gradient, is $\omega'^2 \sim \omega_0^2 R^2/D^2$. The small parameter $(R/D)^2$ measures both the area fraction covered by the vortices and controls the extent of the tails of the p.d.f.s of the gradients, since the strongest gradients are those inside the vortex cores, and are $O(\omega_0)$, while it follows from the previous estimate that $\omega_0/\omega' = O(D/R)$. It is also clear that most of the gradients that are stronger than ω' but weaker than $O(\omega_0)$ correspond to points outside the cores, so that even the intermittent tails are predominantly irrotational. The cores themselves behave like point vortices except in a very small fraction of the area. The same can be said of the p.d.f.s of the velocity components although, as will be seen below, their weaker dependence with distance makes the tails of their p.d.f.s less pronounced.

Consider first the gradients. The following argument, adapted from Feller (1971, p. 179), shows that, in the limit of a two-dimensional velocity field generated by numerous point vortices, their p.d.f.s have algebraic tails. The only characteristic distance in the problem is the mean vortex separation D, and it follows from dimensional analysis that the p.d.f. of the gradients can only depend on the dimensionless group $D^2 s/\Gamma$, where s is any component of the velocity gradient, and Γ is the characteristic circulation of each vortex. Distribute the vortices into Q statistically equivalent subgroups, and denote by $s^{(i)}(\boldsymbol{x}), i = 1 \ldots Q$, the random variables representing the velocity gradients generated by each subgroup at the point $\boldsymbol{x}$. The gradient due to the full system is $s(\boldsymbol{x}) = \sum s^{(i)}(\boldsymbol{x})$. The joint system is statistically similar to any one of the subsystems, but its vortex density per unit area is N times larger. This is equivalent to decreasing vortex separation by a factor $Q^{-1/2}$ and to re-scaling the gradients by a factor Q. The result is that the probability distribution satisfies

$$p\left(\sum s^{(i)}\right) = p(Q^{1/\alpha} s^{(i)}), \tag{2.1}$$

with $\alpha = 1$. This equation characterizes a member of the family of *stable* probability distributions, each of which is defined, except for scaling constants, by the exponent α. Their properties are described in detail by Feller (1971), to which the reader should refer for a full treatment, and they act as limit points for the addition of variables with the right probability densities. More precisely, a stable distribution of degree α is the limit for the sum of mutually independent random variables having common

distributions whose incomplete second moments

$$\mu_2(s) = \int_{-s}^{s} x^2 p(x)\,\mathrm{d}x \sim s^{2-\alpha} \quad \text{when} \quad s \to \infty. \tag{2.2}$$

Both definitions are equivalent and imply, roughly, that the distributions of the individual variables and of their sum have algebraic tails $p(s) \sim s^{-(\alpha+1)}$. In essence, the tails of the probability distributions of the sum are dominated by the contributions of individual strong events, which occur seldom enough that they do not interact with each other, while the central part represents the cancellation of many weaker events, and looks 'Gaussian'. Stable distributions exist only for $0 < \alpha \leqslant 2$, and the particular case $\alpha = 2$ is the Gaussian, for which the classical result is the well-known central limit theorem for distributions with finite variance. That is the only case in which all the moments of the resulting distribution are finite.

The argument given above for the scaling of the p.d.f. can also be put in terms of the behaviour of the probability tails for a single vortex. Consider the transversal or longitudinal velocity gradient generated by a single point vortex at a given point, $s(\boldsymbol{x} - \boldsymbol{x}_0)$. If the location, $\boldsymbol{x}_0$, of the vortex is random, the gradient at point $\boldsymbol{x}$ is itself a random variable, with a probability distribution which is proportional to the fraction of the area occupied by gradients in $(s, s + \mathrm{d}s)$. Since the magnitude of the velocity gradient generated by a vortex is proportional to r^{-2}, where r is the distance to the vortex centre, the area covered by gradients with magnitude greater than s is $A(s) \sim r^2 \sim s^{-1}$, and the probability density for s is $\mathrm{d}A/\mathrm{d}s \sim s^{-2}$. The velocity gradient of the complete flow, generated by a large number of point vortices at random locations, is the sum of the individual gradients due to each vortex, and has the probability distribution of the sum of a large number of individual random variables which, since their tails behave as s^{-2}, approaches the stable distribution with $\alpha = 1$.

The unique stable distribution with $\alpha = 1$, with the extra restriction of symmetry with respect to $s = 0$, is Cauchy's (Feller 1971)

$$p(s) = \frac{c}{\pi(c^2 + s^2)}, \tag{2.3}$$

which should therefore be satisfied both by the longitudinal and by the transversal gradients, $s_{11} = \partial u_1/\partial x_1$ and $s_{12} = \partial u_1/\partial x_2$.

Because of the arguments used to derive it, that distribution can only be expected to apply to the irrotational gradients found outside the coherent vortices, and the extreme ends of the p.d.f.s cannot be derived from it. On the other hand, as argued at the beginning of this section, those gradients include most of the p.d.f., including the tails, and it should be noted that, for them, the argument is independent of the distribution of sizes and circulations of the vortices and that, in the point-vortex limit, it predicts the full p.d.f..

The only requirement for the previous argument is that the distribution of the vortices is such that they can be separated into a large number of classes, each of which is statistically equivalent to the whole. This can be implemented in many ways, but the simplest is to consider all the vortices as being identical, uncorrelated and identically distributed. In this case the theory can be carried further and be made quantitative, and this is the only case that will be considered in the rest of the paper. It should be remembered, however, that the qualitative prediction of (2.3), with some unknown coefficient c, does not require mutual independence and should apply to more general cases.

An elementary analytical derivation of (2.3) in the uncorrelated case is the following. Consider N independent random variables with distributions which we will assume to be symmetric about $x = 0$, and denote the distribution of their sum by $p_N(x)$. The distribution of the sum of two independent variables is the convolution of their individual distributions and, if we define the characteristic function as

$$\phi_N(k) = 2\int_0^\infty \cos(kx)p_N(x)\,\mathrm{d}x, \tag{2.4}$$

the characteristic function of the sum is the product of the two individual characteristic functions. The composite p.d.f. can then be obtained by the inverse Fourier formula,

$$p_N(x) = \frac{1}{\pi}\int_0^\infty \cos(kx)\phi_N(k)\,\mathrm{d}k. \tag{2.5}$$

If we repeat the reasoning that led to (2.1), but separate the N original vortices into two groups of size N_1 and N_2, the dimensional argument implies that the characteristic function can depend only on $\Gamma k/D^2$, which is proportional to kN. The composition rule for the characteristic functions is then

$$\phi_s(k[N_1 + N_2]) = \phi_s(kN_1)\phi_s(kN_2), \tag{2.6}$$

from which it follows that $\phi_s(k) = \exp(-ck)$. The exponential behaviour can either be recognized by inspection, or derived by letting $N_2 \ll N_1$, reducing (2.6) to a differential equation for $\log(\phi_s)$. Equation (2.3) follows by Fourier inversion.

Similar arguments can be used for other variables, as long as they can be computed as the linear superposition of the effects of individual vortex cores. For example, since the velocity scales only with the first power of the vortex separation, the p.d.f. for each velocity component should be stable, with an exponent $\alpha = 2$. The characteristic function satisfies

$$\phi_u(k[N_1 + N_2]^{1/2}) = \phi_u(kN_1^{1/2})\phi_u(kN_2^{1/2}), \tag{2.7}$$

and $\phi_u(k) = \exp(-ck^2)$, corresponding to a Gaussian p.d.f.. In general, the characteristic function of a symmetric stable distribution, with exponent α, can be shown in this way to be $\phi = \exp(-ck^\alpha)$.

As with the gradients, it can also be argued that the velocity generated by a single vortex behaves as r^{-1}, so that the area in which the velocity magnitude is greater than u is proportional to $r^2 \sim u^{-2}$, and the probability density is proportional to $p(u) \sim u^{-3}$. Equation (2.2) cannot be used directly for this distribution, since the incomplete second moment diverges logarithmically with the cutoff, but it is known that the limit is Gaussian (Feller 1971, p. 578). The classical formulation of the central limit theorem assumes that the N individual distributions have finite variance, and the usual estimate that the limit is approached as $N^{-1/2}$ assumes that the third moment also exists. The case of u^{-3} tails is marginal, and represents the most intermittent distribution whose sum still converges to Gaussian, suggesting that the convergence to the limit as a function of N will be slower than in the classical case.

Random variables with no finite variance have not been used often in physics, although they are probably quite common. The argument cited above from Feller (1971) was originally applied to the distribution of the gravitational field in stellar clusters, and can be found in an earlier form in Chandrasekhar (1943). While the present paper was being reviewed, a referee made us aware of an application in the context of spin glasses (Cizeau & Bouchad 1993), and a problem which has been studied quite often is Brownian motion in which the individual steps have stable

probability distributions ('Lévy flights'). It is reviewed in Bouchad & Georges (1990). Lévy flights are also well known in economics (Mandelbrot 1982).

3. The effect of a finite number of vortices.

While there is a well-developed theory for the rate of convergence of the distribution of sums of variables with finite moments, as a function of number of summands, the corresponding theory for general stable distributions is not easily found in the literature, although Feller (1971, §XVI) gives general methods from which it can be derived. We will obtain in this section expansions for the two cases $\alpha = 1$ and 2.

Assume N identically distributed symmetric random variables, with distribution $p(\cdot)$ and characteristic function $\phi(k)$, and define $\phi_N(k)$ as the characteristic function of the p.d.f. of the sum, $p_N(\cdot)$, which satisfies

$$\phi_N(k) = \phi^N(k). \tag{3.1}$$

Because of the positivity of the probability functions and their normalization to unit mass, $\phi(0) = 1$ and, for continuous densities, $\phi < 1$ everywhere else. As a consequence, only the neighbourhood of $k = 0$ is important in the Fourier integral (2.5) for large N, and the limiting distribution for many summands can be studied from the series expansion of $\phi(k)$ for small k which, in turn, is dominated by the behaviour of the tails of $p(x)$.

Consider first the case of the gradients, and assume that

$$p(s) = a_s s^{-2} + o(s^{-3}). \tag{3.2}$$

The constant a_s is a characteristic scale for the gradients, and an asymptotic expansion of ϕ can be obtained for $0 \leqslant ka_s \ll 1$ by separating the integral (2.4) into $(0, a_s)$ and (a_s, ∞), and estimating each part separately. After some work,

$$\phi(k) = 1 - \pi k a_s + O(k^2). \tag{3.3}$$

The expansion for ϕ_N is obtained by noting that $\log(1+\epsilon)^N = N\log(1+\epsilon) = N\epsilon + O(N\epsilon^2)$, so that

$$\phi_N(k) = \exp[-N\pi k a_s + O(Nk^2)]. \tag{3.4}$$

We define a scaled variable $Z \equiv N\pi k a_s$, which is $O(1)$ in the range in which the exponential in (3.4) is significant. The remainder term in the exponent is small, and the exponential can be expanded in series

$$\phi_N(k) \approx \mathrm{e}^{-Z}[1 + O(Z^2/N)], \tag{3.5}$$

and substituted in (2.5) to obtain

$$p_N(s) = \frac{1}{c_N \pi} \int_0^\infty \mathrm{e}^{-Z} \cos(Zs/c_N)\, \mathrm{d}Z\, [1 + O(1/N)] \approx \frac{c_N/\pi}{c_N^2 + s^2} + \cdots, \tag{3.6}$$

where

$$c_N = N\pi a, \tag{3.7}$$

and the residual term is $O(N^{-1})$.

The expansion for the characteristic function in the case of the velocities, for which the tails of the one-vortex distribution behave as

$$p(u) = a_u^2 u^{-3} + O(u^{-4}), \tag{3.8}$$

is similar, but the leading term in ϕ_N is

$$\phi_N(k) \approx \exp[Nk^2 a_u^2(\log ka_u - Q_2) + \cdots], \tag{3.9}$$

where

$$Q_2 = \frac{1}{a_u^2}\left[\int_0^{a_u} u^2 p(u)\,\mathrm{d}u + \int_{a_u}^{\infty} u^2[p(u) - a_u^2 u^{-3}]\,\mathrm{d}u\right] + \tfrac{3}{2} - \gamma, \tag{3.10}$$

and γ is Euler's constant. This is a dimensionless parameter, and is typically $O(1)$. The scaled variable is now $Z \equiv Aka_u$, where A satisfies

$$A^2 = N(Q_2 + \log A). \tag{3.11}$$

This equation only has a solution when N is large enough that $N^{1/2}\exp(Q_2) > 2.33$, in which case it has two roots, the relevant one being

$$A = O(N^{1/2}). \tag{3.12}$$

In terms of the scaled variable

$$\phi_N(k) \approx \exp\left[-Z^2\left(1 - \frac{\log Z}{Q_2 + \log A}\right)\right]. \tag{3.13}$$

The leading term is $\exp(-Z^2)$, which corresponds to a Gaussian distribution for $p_N(u)$, in the limit $N \gg 1$:

$$p_N(u) \approx \frac{1}{(2\pi)^{1/2}\sigma_u}\exp(-u^2/2\sigma_u^2) + \cdots, \qquad \sigma_u = \sqrt{2}Aa_u, \tag{3.14}$$

but the residue is only $O(1/\log A) = O(1/\log N)$, which decays much more slowly than in the previous case, and is actually so slow as to make convergence irrelevant in most practical cases. Moreover, while the series in (3.5) was uniformly valid for $Z \leqslant O(1)$, the one in (3.13) fails near the origin when $Z = O(A^{-1})$. Since the behaviour of a Fourier integral at large u is controlled by the behaviour of the integrand at small k, this failure suggests that the convergence of the far tails of $p_N(u)$ to Gaussian might be even slower than that suggested by the magnitude of the residue, and that there might be a persistent large deviation failure at all N.

In fact, near the origin $\phi_N(k) \approx 1 + Nk^2 a_u^2 \log(ka_u)$, and $p_N(u)$ is dominated at large u by the logarithmic singularity at $k = 0$, whose Fourier transform can be written directly as (Lighthill 1958)

$$p_N(u) \approx Na_u^2 u^{-3}, \tag{3.15}$$

which recovers the cubic tails. In terms of the normalized variable

$$\sigma_u p_N(u) \approx (u/\sigma_u)^{-3}/2(\log A + Q_2) \approx (u/\sigma_u)^{-3}/\log N, \tag{3.16}$$

displaying the logarithmic character of the approximation. The tails become prominent beyond the point at which the Gaussian and (3.16) are of the same order, which is $u/\sigma_u = O(\log^{1/2} \log N)$. This point tends to infinity even slower than the decay of the residue, showing that the algebraic tails remain visible in p_N for all reasonable values of N. We will see in the next section that this last conclusion is modified significantly when the point vortices are substituted by spread Gaussian cores.

An intuitive interpretation of these distributions is possible. The only length scales in the p.d.f.s for a single vortex are contained in the parameters a_s and a_u, which are related to the size of the domain in which the vortex is located. Consider, to fix ideas, the gradients due to a single point vortex of circulation Γ, at the centre of a square box of area L^2. We know that $p(s) \approx a_s/s^2$, and that the probability of finding

gradients stronger than s is $P(s) \approx \int_{|z|>s} p(z)\,\mathrm{d}z = 2a_s/s$. If we apply this equation to the weakest gradient in the box, which is $O(\Gamma/L^2)$, we cover the whole area and we should get an accumulated probability of order one. In this way we estimate that $a_s \sim \Gamma/L^2$. The precise value of a_s can be found by computing the area $A(s)$ covered by gradients larger than a given threshold and letting $p(s) = -L^{-2}\mathrm{d}A/\mathrm{d}s$. The same argument can be applied to the velocity components, and the detailed results are

$$a_u = \frac{\Gamma}{2(2\pi)^{1/2}L}, \qquad a_s = \frac{\Gamma}{2\pi L^2}. \tag{3.17}$$

The process of computing the distributions for the sum of N vortices introduces a new length scale, which is the mean distance between the vortices

$$D = LN^{-1/2}. \tag{3.18}$$

In the case of the gradients, the width of the Cauchy distribution (3.6) is $c_N \sim Na_s \sim \Gamma/D^2$, which is the characteristic gradient at the distance D. In the case of the velocities, the central Gaussian (3.14) has a standard deviation $\sigma_u \sim N^{1/2}a_u \sim \Gamma/D$, which is also the characteristic velocity at that distance. The intuitive interpretation is that gradients, or velocities, which are weaker than those thresholds, and which therefore correspond to points which are farther from the nearest vortex than the mean distance D, contain contributions from many cores, and are 'Gaussianized'. Stronger gradients belong to points in the immediate neighbourhood of one vortex, and which are predominantly influenced by it. They have distributions which are algebraic, similar to those generated by a single vortex, but their proportionality constants are N times larger, because they originate in N independent neighbourhoods, instead of in a single one. It is easy to see from (3.6) and (3.7) that the behaviour of the tail of the distribution of the gradients is $p_N(s) = Na_s/s^2$, which is N times larger than for a single vortex, while (3.15) can be interpreted in the same way for the velocities. Figure 1 summarizes this decomposition for two particular cases of gradients and velocities, while figure 2 displays the evolution of both distributions as a function of the number of vortices. The one-vortex p.d.f.s in these figures are chosen arbitrarily, with the appropriate tail decay laws, while the N-vortex ones are computed numerically by Fourier convolution, as in (2.5)–(3.1).

The different behaviours of the two limits are clearly displayed in those figures. For the velocities the convergence is slow and the algebraic tails are strong even for $N = 10^4$, while the distribution of the sum in the case of the gradients is indistinguishable from the Cauchy limit for $N = 10$.

4. The effect of extended cores

In the point vortex model, the velocity and the gradients are unbounded at the vortices, and the tails of the p.d.f.s extend to infinity. In actual turbulence the vortices have spread cores, with a vorticity distribution that is approximately Gaussian (McWilliams 1990), and the maximum values of the different quantities are determined by the size of the cores. It turns out that a sharp tail cutoff is a reasonable model for the modifications introduced by the Gaussian core in the probability distributions of a single point vortex (see figure 3). Since we will always assume that the vortices are small with respect to the box, and even with respect to their mean separation, the presence of extended cores affects little the behaviour of the probability tails below the cutoff, but the presence of the latter is important in determining the statistical

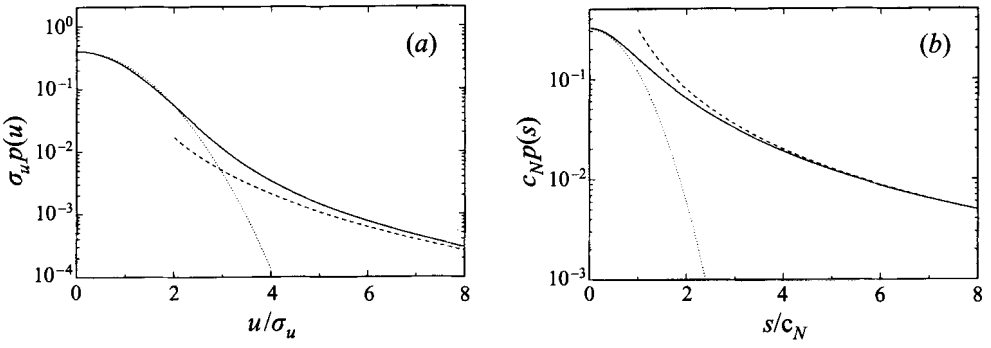

FIGURE 1. Decomposition of the p.d.f. of the sum of $N = 100$ identical vortices, showing the osculating Gaussian (dotted line) and the tails (dashed), using values from the equations in the text. The solid lines are the full p.d.f.s, obtained by numerical convolution. (*a*) Velocities, initial p.d.f.: $p(u) \sim [1 - \exp(u^4/\pi^4)]/u^3$ (see figure 2). (*b*) Gradients, initial p.d.f.: $p(s) \sim [1 - \exp(s^4/\pi^4)]/s^2$.

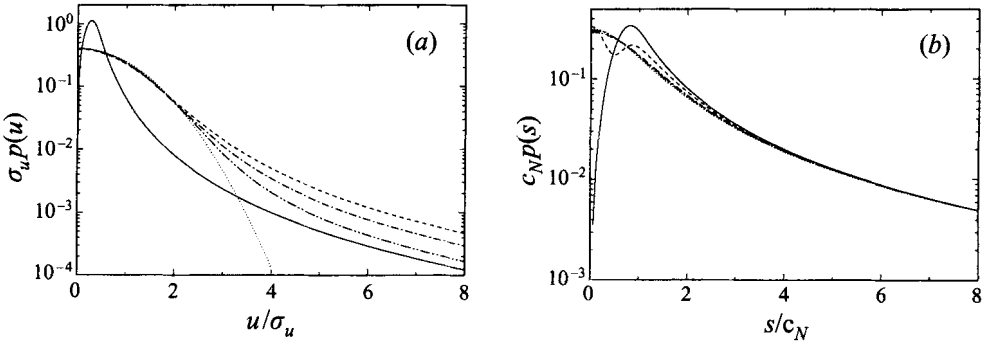

FIGURE 2. Probability distribution functions for sums of N identical independent variables, obtained as in figure 1. (*a*) Velocities. Solid line: $N = 1$; dashed: 10; dash-dot: 10^2; dashed-double-dotted: 10^4; dotted: Gaussian. All curves scaled by (3.11), (3.14), except for $N = 1$, whose scaling is arbitrary. (*b*) Gradients. Solid line: $N = 1$; dashed: 2; dash-dot: 5; dashed-double-dotted: 10; dotted: Cauchy's; scaled by (3.7). The last three lines can barely be distinguished.

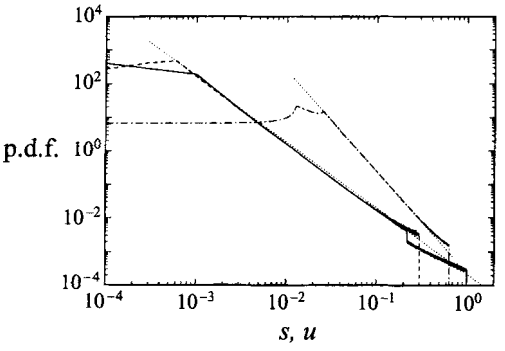

FIGURE 3. P.d.f.s for a single Gaussian vortex core, located at the centre of a square box of side $L = 80$. Solid line: s_{12}; dashed: s_{11}; dash-dotted: velocity. The two dotted lines are power laws with the coefficients from (3.17).

moments. In fact, both for the velocity and for the gradients, a finite cutoff of the tails is needed to define variances for the distributions.

The p.d.f.s in figure 3 were obtained numerically for a vorticity distribution

$$\omega = \omega_0 \exp(-r^2/R^2), \tag{4.1}$$

with $\omega_0 = 2$ and $R = 1$, located at the centre of a large square box. The dotted lines are the p.d.f.s of a point vortex in the same box, with the coefficient given by (3.17). They only differ from the computed ones at very low gradients, where the effect of the box has not been included in the point vortex case, and near the sharp cutoffs, which correspond to the behaviour inside the core. The discontinuity in the tail of the p.d.f. for s_{12} is due to the artificial symmetrization of the distribution, which reflects the presence of vortices of both signs. The p.d.f. of a single vortex is not symmetric, and the step corresponds to the cutoff of the shorter leg.

Once the extended cores are included in the analysis, the core radius, R, defines a third length scale. The limit of large N corresponds to $D \ll L$, and the point vortex limit to $R \ll D$. When both conditions are satisfied, the distributions look like those in the previous section, but the tails are limited to values below those found in individual cores. In fact, since $R \ll D$, the cutoffs affect only the tails of the distributions, where the interaction between cores is negligible, and the structure of the p.d.f.s in their neighbourhood is approximately preserved. If we denote by z_m the cutoff for a given variable z, which is always associated with the core and with the length scale R, and by z_D the corresponding value at a distance D, which defines the width of the 'Gaussian' region, the extent of the tail is z_m/z_D. In our two cases

$$\frac{u_m}{u_D} \approx \frac{D}{R} = \frac{L}{R} N^{-1/2}, \qquad \frac{s_m}{s_D} \approx \left(\frac{L}{R}\right)^2 N^{-1}. \tag{4.2}$$

A useful parameter, which we will use from now on to characterize this ratio, is the area fraction

$$\epsilon = \frac{\pi R^2 N}{L^2}. \tag{4.3}$$

Within the approximations in the previous section, the length of the tails of a given distribution should depend only on this parameter, and (4.2) implies that, for the gradients, the relative length of the tails is $O(\epsilon^{-1})$, while for the velocity it is shorter, $O(\epsilon^{-1/2})$.

In the case of Gaussian cores, the maximum values of the two gradients and of the velocity are

$$s_{m11} \approx 0.15\omega_0, \qquad s_{m12} = \omega_0/2, \qquad u_m \approx 0.32\omega_0 R, \tag{4.4}$$

from which it follows that the transversal gradients have, in general, the most intermittent tails, followed by the longitudinal ones, and finally by the velocities.

This is tested in figures 4 and 5, which display p.d.f.s obtained numerically by the convolution of those for a single Gaussian vortex. In figure 4 we present results for s_{11}, which very quickly approach a truncated Cauchy distribution, as was the case with point vortices. Note that the slight overshoot near the cutoff was already present in the single-vortex distribution in figure 3. For figure 4, the distributions were normalized using the theoretical estimations in (3.6) and (3.17), and the calculations were repeated, at the same values of ϵ, for two different cases corresponding to $L/R = 200$ and 80. Although the caption in the figure refers to the bigger box, the p.d.f.s for both cases are indistinguishable at the scale of the plot.

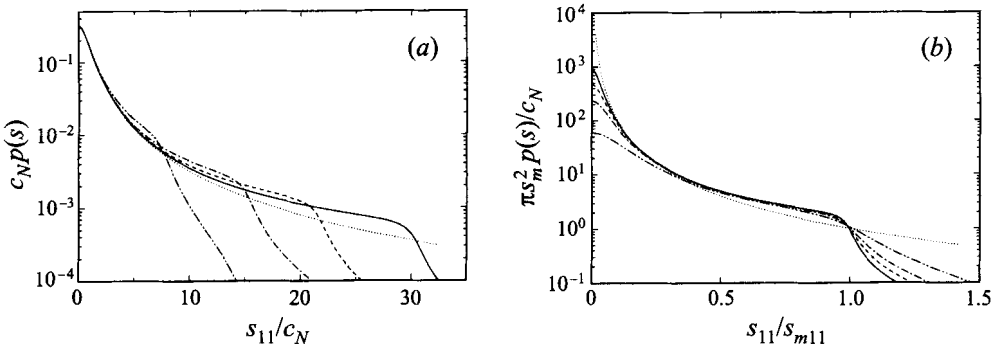

FIGURE 4. P.d.f.s for s_{11}, obtained numerically by convolution of Gaussian vortex cores. In (*a*) the p.d.f.s are normalized as in (3.6), and the dotted line is Cauchy's. In (*b*) they are normalized to emphasize the tails and the constancy of the cutoff. The dotted line is s^{-2}. In all cases $L/R = 200$ for the single-vortex distribution. Solid line: $N = 125$, $\epsilon = 0.0098$. Dashed: $N = 175$, $\epsilon = 0.014$. Dash-dotted: $N = 250$, $\epsilon = 0.020$. Dash-double-dotted: $N = 500$, $\epsilon = 0.039$.

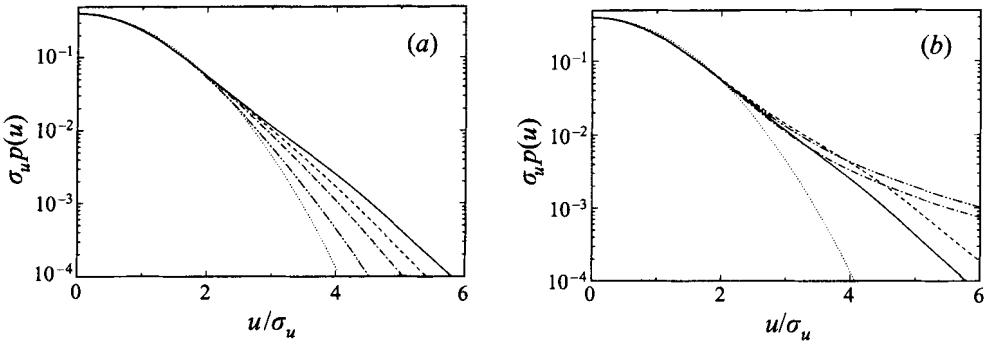

FIGURE 5. Velocity p.d.f.s, obtained numerically by convolution of Gaussian vortex cores. P.d.f.s are normalized using σ_u from (3.11), (3.14). The cases (*a*) are the same as in figure 4, and the dotted line is the osculating Gaussian. In (*b*) we compare two cases at same ϵ but for a different number of vortices, as well as the corresponding point vortex distributions. Solid line: $N = 125$, $\epsilon = 0.0098$, $L/R = 200$. Dashed: $N = 20$, $\epsilon = 0.0098$, $L/R = 80$. Dash-dotted: $N = 125$, $\epsilon = 0$. Dash-double-dotted: $N = 20$, $\epsilon = 0$.

The same is not true for the velocities, owing to the much slower convergence of the expansion. In figure 5 we plot velocity p.d.f.s obtained for the same cases as in the previous figure. In figure 5(*a*) we present results for the larger box, normalized using the standard deviation computed from (3.11)–(3.14), and the collapse of the central parts is excellent. In figure 5(*b*), we compare the results for the two values of L/R, at the same ϵ and, even if the central parts still collapse, the tails do not. Recall in this connection that the whole Cauchy distribution is the large-N limit in the case of the gradients, while the only part of the velocity p.d.f. which corresponds to the limit is the central Gaussian.

When the velocity p.d.f.s for spread cores are compared in figure 5(*b*) to those for the same number of point vortices, their interpretation as algebraic tails with a smoothed cutoff becomes plausible. In the absence of this direct comparison the algebraic interpretation of the tails would be difficult, and it would only become obvious again for values of ϵ much smaller than those in our sample. This is due to the weaker dependence of the length of the tail as a function of ϵ, compared to the case of the gradients. The shorter tail is masked by the smoothed cutoff, which has

a width comparable to that of the central Gaussian. This last observation can easily be understood if we remember that $p_N(u)$ is the convolution of $p_{(N-1)}(u)$ and $p(u)$, and that any sharp feature in the one-vortex p.d.f. is immediately smoothed by its convolution with the wide central Gaussian of the sum. The same effect is obvious in the structure of the cutoff for the gradients in figure 4 but, there, the longer tails are still clearly visible. The result of all this is that, for the velocities, the behaviours of the point vortices and of the extended cores are very different. While the former, with its infinite velocities near the cores, gives rise to persistent tails, the latter converges fairly rapidly to smoother distributions.

In essence, the difference in the behaviour of the gradients and of the velocities derives from the different ranges of the two quantities. While the gradients are fairly local, decaying as $1/r^2$, and the tails of the p.d.f. persist even in the presence of many vortices, the velocities, which decay like $1/r$, have longer ranges, and even the relatively strong velocities in the neighbourhood of one core are Gaussianized by the influence of their neighbours. Note that this argument does not hold for point vortices, in which the infinite velocities at the centres cannot be compensated by any amount of interaction with a finite number of other vortices.

5. Numerical experiments

In this section we compare the theoretical results obtained above to the evolution of the p.d.f.s of the gradients and velocity components in a numerical simulation of isotropic decaying two-dimensional turbulence in a periodic box (Arroyo *et al.* 1994). The code is fully spectral and dealiased, and the power spectrum is reasonably well resolved after $u't/L \approx 0.2$, with a clear exponential dissipative range at the maximum numerical wavenumber $k_{max} = 341$. It uses fourth-order hyperviscosity, $\nu_4\nabla^4$, with a large scale Reynolds number $u'L^3/\nu_4 = 5 \times 10^{10}$, where u' is the mean-squared value of one velocity component. The initial conditions are chosen so as to duplicate the simulation described in McWilliams (1990) at a somewhat higher resolution. The initial vorticity is random, with a fairly peaked spectrum and Gaussian p.d.f.s, but intermittent tails develop immediately for the gradients. The isotropy relations

$$\langle s_{12}^2 \rangle = 3\langle s_{11}^2 \rangle = 3\omega'^2/8, \tag{5.1}$$

are well satisfied at all times, where $\langle\cdot\rangle$ stands for averaging over the whole box and $\omega'^2 = \langle\omega^2\rangle$. Note that none of the p.d.f.s of the point vortex model has finite variance, so that the existence of all the averages in (5.1) depends on the parameters of the extended cores, and that the same is true for u'.

An algorithm was developed to identify individual vortices (Jiménez, Moffatt & Vasco 1996), and it was used to compute vortex numbers and area parameters at four times during the decay of the flow, whose properties are summarized in table 1. It fits an elliptical Gaussian vorticity distribution to each core, to obtain the core geometry and circulation. The fourth column in the table compares the total flow enstrophy with that contained in the vortices identified by the algorithm, and it is clear that most of the enstrophy quickly becomes concentrated in the cores. The next two columns give values for the area parameter ϵ. One of them, S_v/L^2, is computed directly from the vortex catalogue, while the other is computed from the relation

$$\epsilon = \omega'^4/\langle\omega^4\rangle, \tag{5.2}$$

which can easily be shown to be true for identical non-interacting Gaussian cores.

	$u't/L$	N	$\omega_v'^2/\omega'^2$	ϵ	S_v/L^2	L/R	c_N/ω'	$\sigma_u/\omega' L$
———	0.4	346	0.88	0.045	0.046	155	0.150	0.0087
- - -	1.0	175	0.96	0.032	0.037	131	0.126	0.0097
— · —	2.1	95	1.02	0.023	0.027	113	0.107	0.0105
— · · —	3.7	57	1.02	0.019	0.022	97	0.097	0.0117

TABLE 1. Characteristics of the flows fields used in §5. Line types are used consistently in the figures. The area parameter ϵ is computed both from (5.2), and directly from the vortex catalogue. The former is the one used in the paper. The fourth column compares the enstrophy contained in the vortices identified by the program, $\omega_v'^2$, to the total enstrophy in the field. The slight excess in the last two fields is a measure of error for the Gaussian core model.

The results from both methods are very similar and, since (5.2) is more robust and easier to apply, it will be used below in preference to the direct method.

The number of vortices, N, given in table 1 includes vortices with a rather wide distribution of sizes, which can only be approximately related to the identical cores assumed in §4. The number itself is somewhat uncertain, since an arbitrary decision has to be taken on the minimum size at which an object is considered a vortex, and the total number depends on this threshold. We have decided to keep all vortices compatible with our numerical resolution ($R > 1$ grid point), and our vortex count is approximately 20% higher than that in McWilliams (1990) at the first time considered, but decreases to about the same number as in that paper by the end of the run.

To relate the numerical simulations to the theoretical p.d.f.s we still need to estimate the value of the circulation, or the peak vorticity, in an equivalent population of identical vortex cores. It is easy to show that, for identical Gaussian vortices,

$$\omega_0 = \omega'(2/\epsilon)^{1/2}. \tag{5.3}$$

If ϵ is estimated from (5.2), using (5.3) is equivalent to estimating ω_0 from the fourth moment of the vorticity p.d.f., and ω' from the second. With these definitions we can compute theoretical widths for the Cauchy and Gaussian limits of the distributions, using the equations in the two previous sections,

$$\frac{c_N}{\omega'} = \frac{\epsilon^{1/2}}{\sqrt{2}}, \qquad \frac{\sigma_u}{\omega' L} = \frac{A\epsilon^{1/2}}{N(2\pi)^{1/2}}, \tag{5.4}$$

where A is given by (3.11), and is only a function of N and of the parameter Q_2 from (3.10). The latter is a function of the one-vortex p.d.f. at low velocity magnitudes, and it depends only on the geometry of the box. It can be computed numerically and, for a small vortex in a periodic box, $Q_2 \approx 0.08$. As a comparison, the result for the simple open box used in §4 is $Q_2 \approx -0.16$. A value for L/R can also be derived from N and from the definition of ϵ. The results are given in the last three columns of table 1. Note in particular that the values for L/R are intermediate to the two cases considered in §4, and that the ϵ are in the less-intermittent range considered there.

Note that, if the approximations (5.2) and (5.3) are accepted, (5.4) is a prediction of the absolute scale of the p.d.f.s for the gradients and for the velocities, with no adjustable parameters. Note also that (5.2) and (5.3) are statements about the vorticity p.d.f., which is not being used directly in this paper. Once the p.d.f.s of numerical flow fields are scaled with (5.4) they can be compared with the normalized Cauchy and Gaussian distributions predicted in the previous sections. The results are given in figures 6–8. The scaling of the central p.d.f.s for both gradients in figure 6 is excellent,

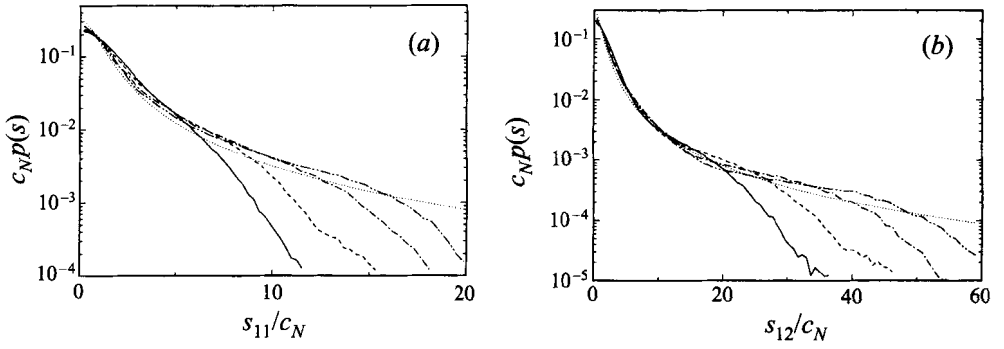

FIGURE 6. Gradient p.d.f.s for the numerical flow experiment described in the text. Lines are as in table 1, and the dotted line is the normalized Cauchy. (*a*) s_{11}. (*b*) s_{12}

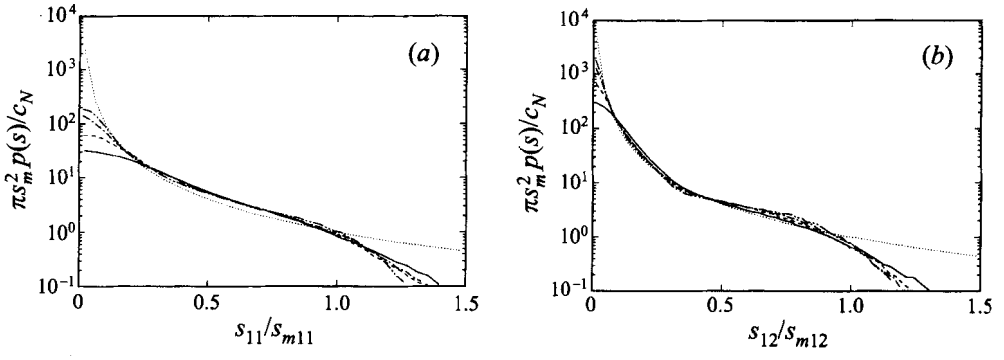

FIGURE 7. Same as figure 6, but with p.d.f.s scaled to emphasize the tails and the influence of the cutoff. Normalization is the same as in figure 4(*b*).

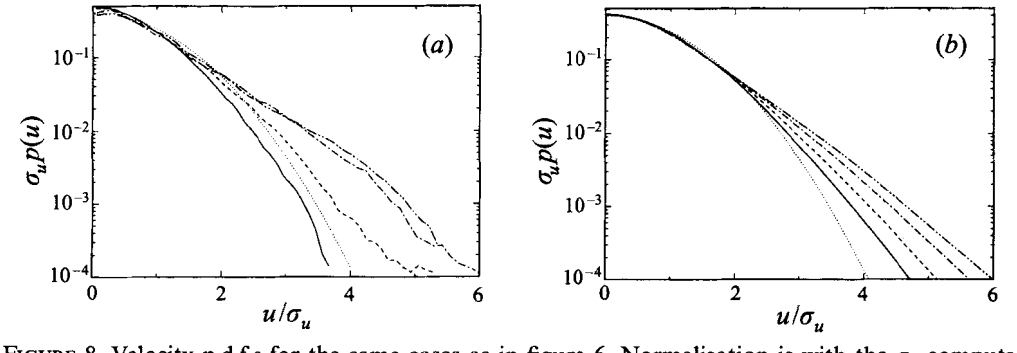

FIGURE 8. Velocity p.d.f.s for the same cases as in figure 6. Normalisation is with the σ_u computed from the run parameters, as explained in text. Dotted line is Gaussian. Scaling should be compared to figure 5(*a*). (*a*) Simulation results. (*b*) Numerical convolution results with the same parameters as the simulations.

even if ω', which is used as the basic scaling parameter, varies by a factor of two during the time of the simulation.

The p.d.f.s for the two gradients also agree well with the normalized Cauchy distribution, and the deviations from it are similar to those in figure 4 for extended Gaussian cores. The four simulations are comparable, in terms of ϵ, to the two leftmost curves for s_{11} in figure 4, and the same overshoot above the Cauchy distribution can be observed in both cases.

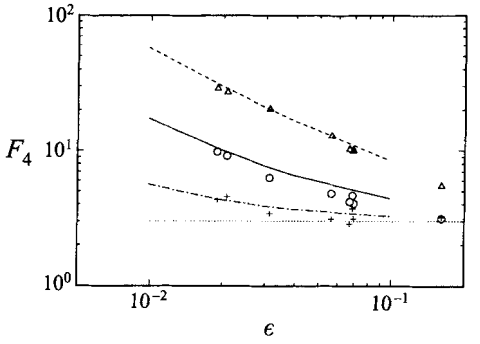

FIGURE 9. Flatness factors for s_{11} (circles and solid line), s_{12} (triangles and dashed line), and velocity (crosses and dash-dotted line). Symbols are from simulations; lines are numerical convolution results at the same ϵ and $L/R = 80$. Dotted line is Gaussian, $F = 3$.

The collapse of the tails in terms of s_m is tested in figure 7, in which the maximum gradients are taken from (4.4) and (5.3). This figure should be compared to figure 4(*b*), and again the collapse is excellent. In particular the p.d.f.s for s_{11} should be compared to the two curves with higher ϵ in figure 4(*b*).

The collapse of the central Gaussians in figure 8(*a*) is satisfactory, specially when it is taken into account that no experimental values of u' were used in that figure. The tails, as has always been the case for the velocity, do not collapse. The p.d.f. at the first time considered is close to Gaussian but, as the decay progresses, the number of vortices decreases and the area ratio becomes smaller, with the result that residual algebraic tails become noticeable. They compare favourably with those in figure 8(*b*), which are computed by numerical convolution of the single-vortex p.d.f. at the values of ϵ and N measured for the simulations. The agreement is specially good for the last three cases, in which the area ratio has decreased enough for the small-vortex limit to become applicable.

A more compact comparison of the behaviour of the predicted and observed tails for all the distributions can be made in terms of the flatness factor

$$F_4 = \mu_4/\mu_2^2, \tag{5.5}$$

which would be equal to 3 for a Gaussian, and infinite for an unbounded Cauchy distribution. Measured and predicted flatness are compiled in figure 9, which includes the simulation described in this section, and other simulations at different Reynolds numbers and stages of developments, using both fourth-order hyperviscosity and Newtonian viscosity. For those other simulations only ϵ was determined, using (5.2), but the number of vortices was not measured. Although that is not important for the gradients, we have seen that it has an influence on the velocities, for which the prediction is, therefore, uncertain. The theoretical results in figure 9 were obtained by numerical convolution of the p.d.f.s in figure 3 but, for the gradients at small ϵ, they can be approximated by those obtained for a Cauchy distribution truncated at s_m,

$$F_4 = \frac{\pi}{3\epsilon}\frac{s_m}{\omega_0} + \frac{\pi^2 - 2}{6} + O(\epsilon). \tag{5.6}$$

For the velocities we have included both the convolution results and the Gaussian limit $F_4 = 3$. As could be expected from the comparison of the p.d.f.s, the agreement is satisfactory, and becomes better for those cases, like s_{12} at low ϵ, with the most intermittent distributions.

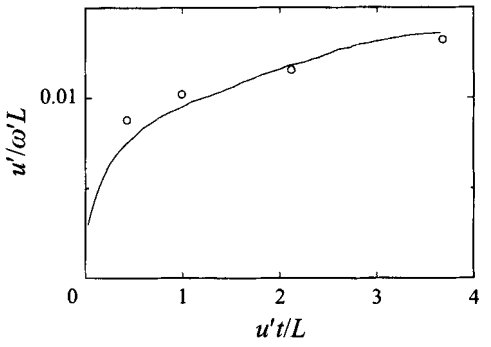

FIGURE 10. Velocity/vorticity r.m.s. ratio for the simulation in the text. Line is simulation results, and symbols are the predictions from the convolution of the single-vortex p.d.f.

Finally figure 10 shows the predicted values of the ratio between r.m.s. velocity and vorticity, and the results of the simulation. The prediction is obtained from the value of u'/σ_u derived from the numerical convolution of the one-vortex simulations, together with (5.4). The agreement is good, specially again for the later times in which the small-vortex limit is applicable. This agreement is interesting, because it tests the central hypothesis of this paper, which is that the geometrical arrangement of the vortices is random. Once we have tested, as in figures 6 and 7, that the parameters chosen for our vortices represent reasonably well the distributions of the gradients, the calculation of the r.m.s. velocity follows immediately from the property that the variance of the sum of mutually independent variables is the sum of individual variances. These truncated distributions all have finite second moments, and the variance of the one-component velocity p.d.f. is the specific kinetic energy of the flow. The agreement in figure 10 is therefore a test that the kinetic energy of the vortex distribution is, statistically, the sum of the kinetic energies due to the individual vortices. It has been suggested that the representation of two-dimensional turbulence in terms of point vortices should take into account screening effects like those found in plasmas (Ruelle 1990), but the present result implies that, at least in this case, such effects are negligible.

6. Conclusions

We have given a simple statistical argument that predicts the form of the p.d.f. of the velocity gradients in decaying two-dimensional turbulence, in the limit in which the flow is dominated by a large number of compact vortices. It turns out to be Cauchy's, which has algebraic tails, and no finite moments, including variance. When the effect of spread Gaussian cores is included, rather than point vortices, the range of the algebraic tails is seen to increase to infinity as the area fraction covered by the vortices goes to zero. The same argument predicts Gaussian distributions for the velocity components. The first prediction is shown to agree well with numerical simulations of decaying turbulence, but the second one does not.

This failure is traced to the different rates of convergence to the limit in both cases, as a function of the number of vortices. While the convergence is algebraic in the first case, it is only logarithmic in the second, and the corrections take the form of new algebraic tails, that persist for all practical situations in the case of point vortices. When the effect of spread cores is included, the range of these tails increases also with decreasing area fraction, but slower than in the case of the gradients, resulting in tails

that, although persistent, are difficult to identify as algebraic, except for unrealistically small vortices.

Once the effects of spread cores and of a finite vortex number are included, the predictions can be compared in detail with the result of turbulence simulations, and the agreement is satisfactory. In particular, the functional forms and the width of all the p.d.f.s are predicted correctly from the measured parameters of the vorticity distribution. There are no adjustable parameters in this comparison, besides the measured values for the number of vortices, radii and circulations.

Besides the assumption that all the vorticity is concentrated in the vortex cores, which is checked independently to be a good approximation for our simulation, the only physical hypothesis in our study is that the arrangement of the vortex cores is random, with no dynamical aggregation or screening effects. One consequence, which was checked explicitly in figure 10, is that the mean kinetic energy is the sum of the kinetic energy due to the vortex cores, and that interaction effects are negligible. It is not clear whether this, which would be an important conclusion for the modelling of two-dimensional turbulence in terms of point vortices, is a general property, or is just true for the particular simulation considered.

It is tempting to apply similar arguments to three-dimensional turbulent flows, which also display intermittency effects at large Reynolds numbers, and in which compact vortex filaments have also been observed. In that case, however, the vortices do not seem to be the dominant source of the velocity gradients, and a similar analysis of the p.d.f.s would require an understanding of all the other components of the flow.

This work was supported by the Human Capital and Mobility program of the European Union, under contract CHRXCT920001. I am grateful for several useful discussions with Joe Keller and Rachel Kuske, at Stanford, on the subject of §3.

REFERENCES

ANSELMET, F., GAGNE, Y., HOPFINGER, E. J. & ANTONIA, R. A. 1984 High-order structure functions in turbulent shear flow. *J. Fluid Mech.* **140**, 63–89.

ARROYO, P., PEDRIZZETTI, G., VASCO, C. & JIMÉNEZ, J. 1995 Statistical properties of decaying two-dimensional turbulence. In *Advances in Turbulence V* (ed. R. Benzi), pp. 11–15. Kluwer.

BATCHELOR, G. K. & TOWNSEND, A. A. 1949 The nature of turbulent motion at large wave numbers. *Proc. R. Soc. Lond.* A **199**, 238–255.

BOUCHAUD, J. P. & GEORGES, A. 1990 Anomalous diffusion in disordered media: statistical mechanisms, models and physical applications. *Phys. Rep.* **195**, 127–293.

BRACHET, M. E., MENEGUZZI, M., POLITANO, H. & SULEM, P. L. 1988 The dynamics of freely decaying two-dimensional turbulence. *J. Fluid Mech.* **194**, 333–349.

CASTAING, B., GAGNE, Y. & HOPFINGER, E. J. 1990 Velocity probability density functions of high Reynolds number turbulence. *Physica* D **46**, 177–200.

CHANDRASEKHAR, S. 1943 Stochastic problems in physics and astronomy. *Rev. Mod. Phys.* **15**, 70–74. (Reprinted in *Selected Papers on Noise and Stochastic Processes* (ed. N. Wax). Dover 1954.)

CIZEAU, P. & BOUCHAUD, J. P. 1993 Mean field theory of dilute spin-glasses with power-law interactions. *J. Phys.* A: *Math. Gen.* **26**, L187–L193.

FELLER, W. 1971 *An Introduction to Probability Theory and its Applications* (2nd Edn), vol. 2, pp. 169–172 and 574–581. Wiley.

GURVICH, A. S. & YAGLOM, A. M. 1967 Breakdown of eddies and probability distributions for small-scale turbulence, boundary layers and turbulence. *Phys. Fluids Suppl.* **10**, S 59–65.

HOSOKAWA, I. & YAMAMOTO, K. 1990 Intermittency of dissipation in directly simulated fully developed turbulence. *J. Phys. Soc. Japan* **59**, 401–404.

JIMÉNEZ, J., MOFFATT, H. K. & VASCO, C. 1996 The structure of the vortices in freely decaying two-dimensional turbulence. *J. Fluid Mech.* **313**, 209–222.

JIMÉNEZ, J., WRAY, A. A., SAFFMAN, P. G. & ROGALLO, R. S. 1993 The structure of intense vorticity in isotropic turbulence. *J. Fluid Mech.* **255**, 65–90.

KAILASNATH, P., SREENIVASAN, K. R. & STOLOVITZKY, G. 1992 Probability density of velocity increments in turbulent flows. *Phys. Rev. Lett.* **68**, 2766–2769.

KERR, R. M. 1985 Higher order derivative correlation and the alignment of small-scale structures in isotropic numerical turbulence. *J. Fluid Mech.* **153**, 31–58.

KOLMOGOROV, A. N. 1962 A refinement of previous hypotheses concerning the local structure of turbulence in a viscous incompressible fluid at high Reynolds number. *J. Fluid Mech.* **13**, 82–85.

LIGHTHILL, M. J. 1958 *Introduction to Fourier Analysis and Generalised Functions*, §4 and table I. Cambridge University Press.

MANDELBROT, B. B. 1974 Intermittent turbulence in self-similar cascades: divergence of high moments and dimension of the carrier. *J. Fluid Mech.* **62**, 331–358.

MANDELBROT, B. B. 1982 *The Fractal Geometry of Nature*, §37. Freeman.

MCWILLIAMS, J. C. 1990 The vortices of two-dimensional turbulence. *J. Fluid Mech.* **219**, 361–385.

MENEVEAU, C. & SREENIVASAN, K. R. 1991 The multifractal nature of the energy dissipation. *J. Fluid Mech.* **224**, 429–484.

NOVIKOV, E. A. 1971 Intermittency and scale similarity in the structure of a turbulent flow. *Prikl. Mat. Mech.* **35**, 266–277.

OBUKHOV, A. M. 1962 Some specific features of atmospheric turbulence. *J. Fluid Mech.* **13**, 77–81.

PARISI, G. & FRISCH, U. 1985 On the singularity structure of fully developed turbulence. In *Turbulence and Predictability in Geophysical Fluid Dynamics* (ed. M. Gil, R. Benzi & G. Parisi), pp. 84–88. North-Holland.

PULLIN, D. I. & SAFFMAN, P.G. 1993 On the Lundgren–Townsend model of turbulent fine scales. *Phys. Fluids* A **5**, 126–145.

RUELLE, D. 1990 Is there screening in turbulence? *J. Statist. Phys.* **61**, 865–867.

RUETSCH, G. R. & MAXEY, M. R. 1991 Small scale features of vorticity and passive scalar fields in homogeneous isotropic turbulence. *Phys. Fluids* A **3**, 1587–1597.

SANTANGELO, P., BENZI, R. & LEGRAS, B. 1989 The generation of vortices in high-resolution, two-dimensional decaying turbulence and the influence of initial conditions on the breaking of similarity. *Phys. Fluids* A **1**, 1027–1034.

SHE, Z.-S. 1991 Intermittency and non-Gaussian statistics in turbulence. *Fluid Dyn. Res.* **8**, 143–159.

SHE, Z.-S., JACKSON, E. & ORSZAG, S. A. 1990 Structure and dynamics of homogeneous turbulence, models and simulations. *Proc. R. Soc. Lond.* A **434**, 101–124.

SIGGIA, E. D. 1981 Numerical study of small scale intermittency in three dimensional turbulence. *J. Fluid Mech.* **107**, 375–406.

TOWNSEND, A. A. 1951 On the fine scale structure of turbulence. *Proc. R. Soc. Lond.* A **208**, 534–542.

VAN ATTA, C. W. & ANTONIA, R. A. 1980 Reynolds number dependence of skewness and flatness factors of turbulent velocity derivatives. *Phys. Fluids* **23**, 252–257.

VINCENT, A. & MENEGUZZI, M. 1991 The spatial structure and statistical properties of homogeneous turbulence. *J. Fluid Mech.* **225**, 1–25.